Contact and Momentum Distribution of the Unitary Fermi Gas by Bold Diagrammatic Monte Carlo

K. Van Houcke,[1,2] F. Werner,[3,2] E. V. Kozik,[4,5] N. V. Prokof'ev,[2,6] and B. V. Svistunov[2,6]

[1] *Department of Physics and Astronomy, Ghent University, Proeftuinstraat 86, B-9000 Ghent, Belgium*
[2] *Department of Physics, University of Massachusetts, Amherst, MA 01003, USA*
[3] *Laboratoire Kastler Brossel, Ecole Normale Supérieure, UPMC, CNRS, 75231 Paris Cedex 05, France*
[4] *Centre de Physique Théorique, Ecole Polytechnique, 91128 Palaiseau Cedex, France*
[5] *Theoretische Physik, ETH Zürich, CH-8093 Zürich*
[6] *Russian Research Center "Kurchatov Institute", 123182 Moscow, Russia*

(Dated: March 26, 2013)

A key observable in strongly interacting resonant Fermi gases is the contact parameter $\mathcal{C}$, which governs both the pair correlation function at short distances and the momentum distribution at large momenta. The temperature dependence of $\mathcal{C}$ was recently measured at unitarity, where existing theoretical predictions differ substantially. We report accurate data for the contact and the momentum distribution in the normal phase of the unitary gas, obtained by Bold Diagrammatic Monte Carlo. In our scheme, $\mathcal{C}$ is extracted from the pair correlation function, while the $\mathcal{C}/k^4$ tail of the momentum distribution, being built in at the analytical level, is free of k-dependent noise.

PACS numbers: 05.30.Fk, 67.85.Lm, 74.20.Fg

The resonant Fermi gas is a fundamental model of quantum many-body physics. It features a smooth crossover between fermionic and bosonic superfluidity, as predicted in the context of condensed matter physics [1–4] and confirmed by remarkable experiments on ultracold atomic Fermi gases near Feshbach resonances [5]. It is also relevant to neutron matter [6] and high-energy physics [7], particularly in the unitary regime reached at the center of the crossover. As a result of the vanishing interaction range, resonant Fermi gases feature characteristic ultraviolet singularities governed by an observable called contact [4, 8–11]. In particular, the density-density correlation function at short distance diverges as

$$\langle\, \hat{n}_\uparrow(\mathbf{r})\, \hat{n}_\downarrow(\mathbf{0})\, \rangle \underset{r\to 0}{\longrightarrow} \frac{\mathcal{C}}{(4\pi\, r)^2} \tag{1}$$

and the momentum distribution has the tail

$$n_\sigma(\mathbf{k}) \underset{k\to\infty}{\longrightarrow} \frac{\mathcal{C}}{k^4}. \tag{2}$$

Here $\mathcal{C}$ is the contact per unit volume for the homogeneous gas, $\hat{n}_\sigma(\mathbf{r}) = \hat{\psi}^\dagger_\sigma(\mathbf{r})\hat{\psi}_\sigma(\mathbf{r})$ is the density operator, and the spin-σ momentum distribution $n_\sigma(\mathbf{k})$ is normalised to $\int n_\sigma(\mathbf{k}) d^3k/(2\pi)^3 = n_\sigma = \langle \hat{n}_\sigma(\mathbf{r})\rangle$. A direct manifestation of Eq. (1) is that in a unit volume, the number of pairs of fermions separated by a distance smaller than s is $\mathcal{C}\, s/(4\pi)$ in the $s \to 0$ limit. Hence $\mathcal{C}$ controls the (anomalously high) density of pairs with vanishing interparticle distance [8, 10, 12].

The contact is directly related to a large variety of observables that have been measured by various experimental techniques: the population of the closed channel molecular state measured by laser molecular spectroscopy [13, 14], the large-momentum tail of the static structure factor measured by Bragg spectroscopy [15–17], the tail of the momentum distribution measured by non-interacting time-of-flight or by momentum-resolved radiofrequency spectroscopy [18], the derivative of the energy with respect to the inverse scattering length [9] extracted from the pressure equation of state measured by in-situ imaging [19], and the large-frequency tail in radiofrequency spectroscopy [18, 20, 21].

The recent experimental study [21], being both locally resolved and temperature dependent, is the first to have access to the temperature dependence of the contact of the homogeneous unitary gas. On the theoretical side, however, current predictions based on summation of certain classes of Feynman diagrams [22–24] or lattice Quantum Monte Carlo simulations [25] differ substantially even at the qualitative level, especially on approach to the superfluid transition from the normal side.

In this Letter, we present controlled accurate results for the contact and the momentum distribution of the unitary Fermi gas in the normal phase, obtained by Bold Diagrammatic Monte Carlo (BDMC). We evaluate the contact $\mathcal{C}$ by expressing it as a density of pairs. We further demonstrate that the momentum distribution obtained within our BDMC scheme features the $\mathcal{C}/k^4$ tail with the same value of $\mathcal{C}$ and without k-dependent statistical noise.

In our BDMC scheme, all Feynman diagrams are stochastically sampled to high order, and abelian resummation is applied to the diagrammatic series [26, 27]. The diagrams are built on single-particle and pair propagators which are bold, i.e. fully dressed. We directly extract the contact from the bold pair propagator Γ thanks to the relation

$$\mathcal{C} = -\Gamma(\mathbf{r} = \mathbf{0}, \tau = 0^-) \tag{3}$$

(we set $\hbar$ and m to unity). This relation is consistent with the interpretation of $\mathcal{C}$ in terms of a density

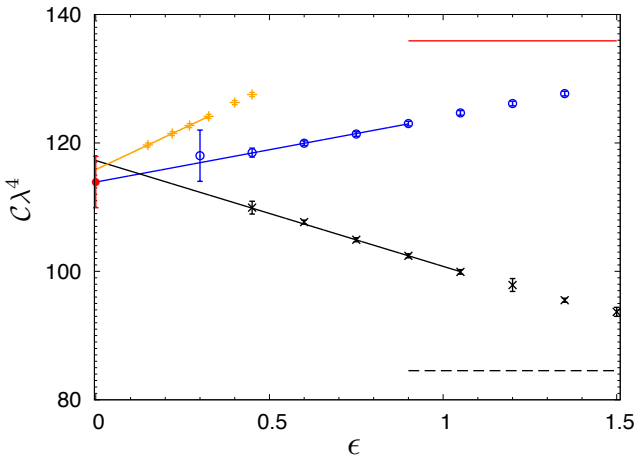

FIG. 1: Resummation of the dimensionless contact $\mathcal{C}\lambda^4$ (at $\beta\mu = 1$). After linear extrapolation to $\epsilon \to 0$, consistent results are obtained by the different resummation methods: Lindelöf ($\circ$), shifted Lindelöf ($\times$), and Gauss ($+$). Also shown are the first order [23] and third order results without resummation (solid and dashed horizontal lines).

of pairs, since it is formally analogous to the relation $n_\sigma = G_\sigma(\mathbf{r}=\mathbf{0}, \tau = 0^-)$ between the single-particle density and the bold single-particle propagator G. Although Eq. (3) was first obtained within T-matrix approximations [24, 28, 29], it is actually exact. A simple way to derive it is to use the regularized version of Eq. (1) which holds in a lattice model [30],

$$\mathcal{C} = {g_0}^2 \, \langle \hat{n}_\uparrow(\mathbf{0}) \, \hat{n}_\downarrow(\mathbf{0}) \rangle \tag{4}$$

i.e. the contact is equal to the double occupancy, up to a renormalization factor set by the bare coupling constant g_0 (see also [12]). The result (3) then follows from the fact that

$$\Gamma(\mathbf{r}, \tau) = g_0 \, \delta(\tau) \frac{\delta_{\mathbf{r},\mathbf{0}}}{b^3} - {g_0}^2 \left\langle \mathrm{T}(\psi_\downarrow \psi_\uparrow)(\mathbf{r}, \tau)(\psi_\uparrow^\dagger \psi_\downarrow^\dagger)(\mathbf{0}, 0) \right\rangle \tag{5}$$

or diagrammatically

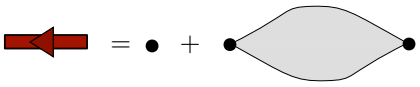

(6)

where T is the time-ordering product, and the first term does not contribute in the continuum limit where the lattice spacing b tends to zero.

We start by verifying the consistency between different resummation methods. As in Ref. [26] we use abelian resummation methods, where the N-th order terms of the series are multiplied by $e^{-\epsilon \lambda_{N-1}}$, with λ_n depending on the resummation method: $\lambda_n = n \ln n$ for Lindelöf, $\lambda_n = n^2$ for Gauss, and $\lambda_n = (n-1)\ln(n-1)$ for shifted-Lindelöf. Figure 1 shows the ϵ-dependence of the dimensionless contact $\mathcal{C}\lambda^4$, for a fixed value of the grand-canonical parameter $\beta\mu$. Here $\beta = 1/(k_B T)$ is the inverse temperature and $\lambda = \sqrt{2\pi\beta}$ is the thermal wavelength. When the regularization parameter ϵ is extrapolated to zero, the three methods give consistent results. To understand the overall shape of the resummation curves and to make a link with the self-consistent T-matrix approximation of Refs. [23, 31], we remark that for $\epsilon \to \infty$, the Lindelöf and Gauss curves would asymptote to the result obtained by truncating the diagrammatic series at order 1 as in Refs. [23, 31], while the shifted-Lindelöf data would tend to the substantially different result obtained by truncating the diagrammatic series at order 3.

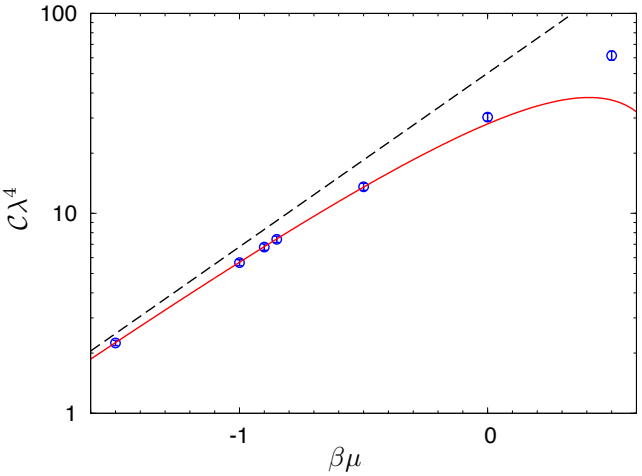

FIG. 2: BDMC results for the contact in the high-temperature regime, compared to the virial expansion [24, 32] at order two (dashed line) and three (solid line).

The temperature dependence of the contact in the high-temperature regime is shown in Fig. 2, where we compare with the virial expansion

$$\mathcal{C}\lambda^4 = 16\pi^2 \left(c_2 \, e^{2\beta\mu} + c_3 \, e^{3\beta\mu} + \ldots \right). \tag{7}$$

The coefficients $c_2 = 1/\pi$ [32] and $c_3 \simeq -0.141$ [24] come from the 2-body and 3-body problem respectively. The agreement with the third-order coefficient c_3 constitutes a non-trivial test of our approach, since this coefficient comes from the three-body propagator [33] which has to be reconstructed in our case by summing an infinite number of diagrams.

The behavior of the contact in the low-temperature region of the normal phase is displayed in Fig. 3. The contact in terms of canonical variables, $\mathcal{C}(n, T)$ or equivalently $\mathcal{C}/{k_F}^4$ *versus* T/T_F, is shown in Fig. 3a. Our results are consistent within error bars with the experimental results of [21]. The lattice Auxiliary Field Quantum Monte Carlo data of Ref. [25] disagree with our data and contain *a priori* unknown systematic errors coming from discretization of space (i.e. finite filling factor) and of imaginary time. In contrast with the non self-consistent T-matrix results of Ref. [22] and the Nozières Schmitt-Rink results of Ref. [24], we do not observe any

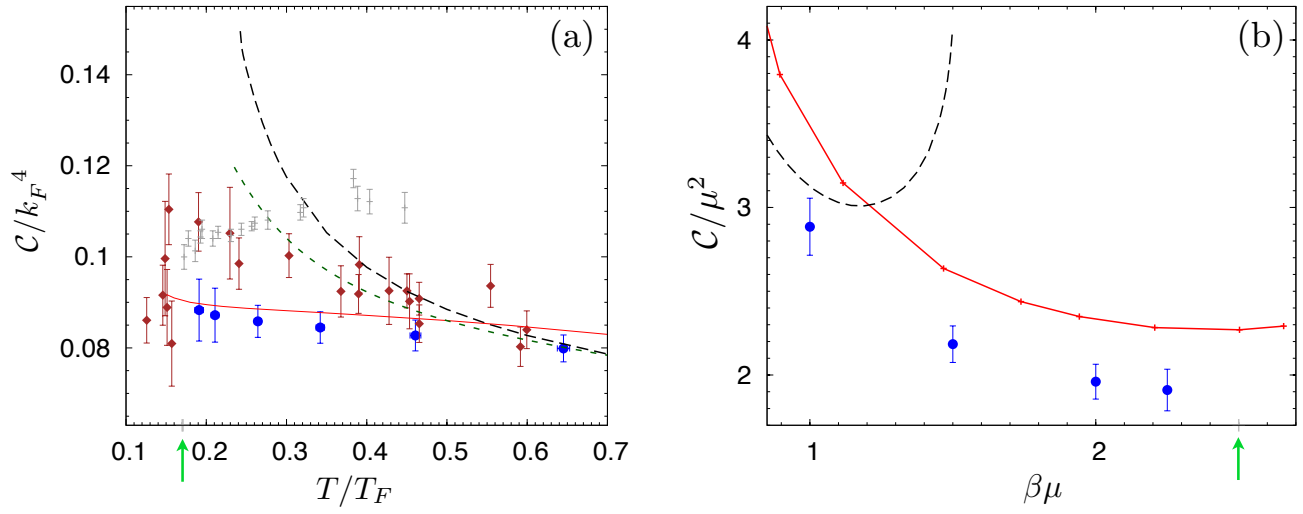

FIG. 3: Temperature dependence of the contact in the low-temperature region of the normal phase, in terms of (a) canonical and (b) grand canonical variables. BDMC (this work): blue solid circles, JILA experiment [21]: brown solid diamonds, lattice AFQMC simulations [25]: grey crosses. The curves correspond to different diagrammatic approximations: non self-consistent T-matrix [22]: dashed black line, self-consistent T-matrix [23]: solid red line, Nozières-Schmitt-Rink [24]: dotted green line in (a) and dashed black line in (b). The transition point to the superfluid phase from Refs. [34, 35] is indicated by the green arrow.

pronounced enhancement when decreasing temperature. The self-consistent T-matrix results of Ref. [23] are remarkably close to our data in Fig. 3a. The contact in terms of grand canonical variables, $\mathcal{C}(\mu,T)$ or equivalently $\mathcal{C}/\mu^2$ *versus* $\beta\mu$, is shown in Fig. 3b. It is natural to use these variables to discuss the different diagrammatic results since the diagrammatic technique is formulated in the grand-canonical ensemble. The functions $\mathcal{C}(n,T)$ and $\mathcal{C}(\mu,T)$ are connected by the equation of state $n(\mu,T)$, given for each of the considered approaches in Refs. [26, 36–38]. The non self-consistent T-matrix and Nozières-Schmitt-Rink approaches yield the same result for $\mathcal{C}(\mu,T)$. Indeed, in both approaches, $\mathcal{C}$ is given by Eq. (3) with Γ replaced by $\Gamma^{(0)}$ which is the sum of the ladder diagrams built on the ideal gas propagators $G^{(0)}$. The self-consistent T-matrix approach overestimates $\mathcal{C}(\mu,T)$ as seen in Fig. 3b, and also overestimates the equation of state $n(\mu,T)$ (see [26]). These two systematic errors largely cancel out when one considers $\mathcal{C}(n,T)$ as in Fig. 3a.

We now turn to the momentum distribution. The large-momentum physics governed by the contact enters in the following way the bold-line diagrammatic formalism (see also [24, 39]). In short, the tail of the momentum distribution comes from the diagram depicted in Fig. 4. More precisely, for $k\to\infty$ the Dyson equation simplifies to $n_\sigma(\mathbf{k}) = G_\sigma(\mathbf{k},0^-) \simeq \int_{-\beta/2}^{\beta/2} d\tau_1 \int_{-\beta/2}^{\beta/2} d\tau_2\, G_\sigma^{(0)}(\mathbf{k},-\tau_1)\Sigma_\sigma(\mathbf{k},\tau_1-\tau_2)G_\sigma^{(0)}(\mathbf{k},\tau_2)$. Here the large-momentum ideal gas propagators $G^{(0)}$ can be replaced by vacuum propagators, which are retarded

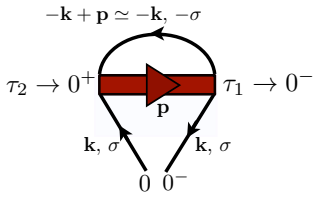

FIG. 4: Leading diagrammatic contribution to the momentum distribution $n_\sigma(\mathbf{k})$ at large k, which can be interpreted physically as the simultaneous propagation of two opposite-spin particles of large and nearly opposite momenta and of a missing pair of lower momentum $p \ll k$. Imaginary time runs from right to left. The single-particle lines propagate forward in time and can be replaced by vacuum propagators. The pair propagator runs backwards in time and is fully dressed.

and quickly decaying functions of imaginary time. Hence the integral is dominated by $\tau_2\to 0^+$ and $\tau_1\to 0^-$, and the imaginary time argument $\tau_1-\tau_2$ of the self-energy tends to 0^-. The behavior of $\Sigma(\mathbf{k},\tau)$ for $k\to\infty$, $\tau\to 0^-$ can be determined analytically by considering the bold diagrammatic series. The lowest-order diagram reads $\Sigma^{(1)}(\mathbf{k},\tau) = \int \frac{d^3p}{(2\pi)^3}\,\Gamma(\mathbf{p},\tau)\,G_{-\sigma}(-\mathbf{k}+\mathbf{p},-\tau)$, where the integral is dominated by momenta $p\ll k$ and the propagator G can be replaced by the vacuum expression $-e^{-\epsilon_k|\tau|}$ in the relevant region $0<-\tau\lesssim 1/k^2\to 0$ (here $\epsilon_k=k^2/2$). As for the higher order bold diagrams, their contribution is suppressed because they include integrations over internal times which are restricted to narrow ranges, since G and Γ become narrow functions

of time at large momentum. Using Eq. (3) we thus obtain

$$\Sigma(\mathbf{k},\tau) \simeq \mathcal{C}\, e^{\epsilon_k \tau}, \quad k \to \infty,\ \tau \to 0^-. \tag{8}$$

After substituting this form into the asymptotic Dyson equation given above, the large-momentum tail, Eq. (2), is recovered.

These analytical considerations have the following implications for our BDMC calculation. Since the $\mathcal{C}/k^4$ tail of the momentum distribution comes exclusively from the lowest-order self-energy diagram, this tail is automatically built into our self-consistent BDMC scheme provided this diagram is evaluated with high precision. We achieve this by using numerical Fourier transformations (rather than Monte Carlo) and analytical treatments of leading-order singularities [27], in the spirit of [31]. Our value of $\mathcal{C}$, of course, still differs from the one of the self-consistent T-matrix approximation of Refs. [23, 31], since our lowest-order diagram is built on the fully dressed pair propagator Γ given by the BDMC self-consistency which includes higher-orders contributions. On the technical side, we note that treating the lowest-order self-energy diagram separately (without using Monte Carlo) has another advantage: the steep function of τ in Eq. (8) would be hard to capture by Monte Carlo sampling.

The momentum distribution multiplied by k^4 is shown in Fig. 5 for our lowest temperature. The large-momentum tail is reproduced without k-dependent statistical noise (in contrast to other Monte Carlo methods [25, 40]) and perfectly agrees with our value of the contact determined from Eq. (3). The momentum distribution for various temperatures is shown in Fig. 6. As the temperature is lowered, we do not observe any incipient discontinuity at k_F, as would be the case for a pronounced degenerate Fermi liquid behavior.

In conclusion, we have incorporated the ultraviolet physics governed by the contact into the framework of BDMC. We accurately evaluated the contact *via* the bold pair propagator. Moreover, our momentum distribution data automatically contain the large-momentum tail with the proper contact coefficient, as we have shown analytically and confirmed numerically. Our data can serve as benchmarks for future experimental and theoretical studies, not only on the contact and momentum distribution themselves, but also in various contexts where the contact appears either in ultraviolet asymptotics [23, 41–44] or in sum rules [8, 42, 45, 46]. We expect that the possibility to incorporate analytical knowledge into BDMC is a generic capability of the approach which will facilitate its applications to other outstanding strongly correlated fermion systems.

Acknowledgements. The data of Refs. [21–25, 36–38] were kindly provided by their authors. This work was supported by Research Foundation Flanders (FWO) (K.V.H.), National Science Foundation grant PHY-1005543, the Optical Lattice Emulator program of the Defense Advanced Research Projects Agency, and a Fellowship for Advanced Researchers from Swiss National Science Foundation (E.K.). Simulations ran on the clusters CM at UMass and Brutus at ETH. Part of this work was done at the Institute for Nuclear Theory, Seattle and the Aspen Center for Physics (programs "Simulations and Symmetries: Cold Atoms, QCD, and Few-hadron Systems", "Fermions from Cold Atoms to Neutron Stars: Benchmarking the Many-Body Problem", "Few- and Many-Body Physics in Cold Quantum Gases Near Resonances"; INT-10-1, INT-11-1, NSF Grant 1066293).

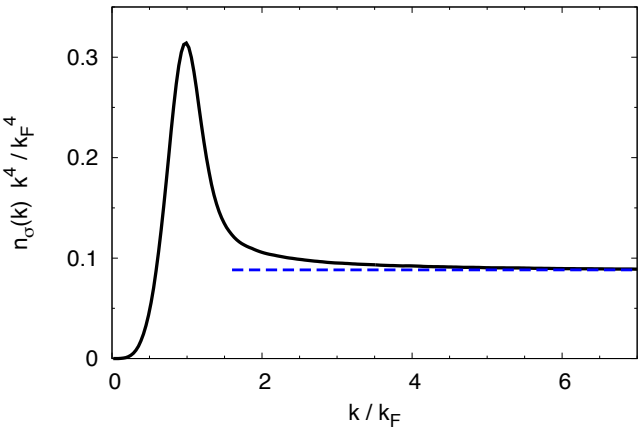

FIG. 5: BDMC data for the momentum distribution $n_\sigma(k)$, multiplied by k^4 in order to reveal the large-momentum tail $n_\sigma(k) \to \mathcal{C}/k^4$. Dashed line: value of the contact $\mathcal{C}$ computed directly from the pair propagator. The temperature is $T/T_F = 0.191(5)$ ($\beta\mu = 2.25$).

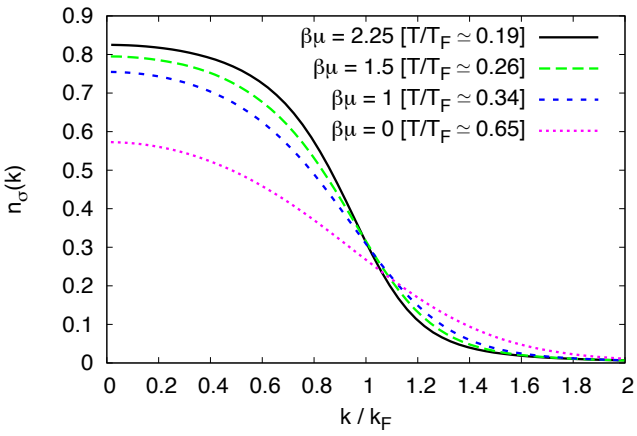

FIG. 6: BDMC data for the momentum distribution at various temperatures.

[1] A. J. Leggett, in: A. Pekalski, J. Przystawa (eds.), *Modern Trends in the Theory of Condensed Matter*, p. 13. Springer, New York (1980).

[2] A. J. Leggett, J. Phys. (Paris) **42**, C7 (1980).
[3] P. Nozières and S. Schmitt-Rink, J. Low Temp. Phys. **59**, 195 (1985).
[4] A. J. Leggett and S. Zhang, Lecture Notes in Physics **836**, 33 (2012).
[5] *The BCS-BEC Crossover and the Unitary Fermi Gas*, Lecture Notes in Physics Volume 836, W. Zwerger ed. (Springer, Heidelberg, 2012).
[6] J. Carlson, S. Gandolfi, and A. Gezerlis, Prog. Theor. Exp. Phys. p. 01A209 (2012).
[7] New J. Phys **14** (2011), *Focus on Strongly Correlated Quantum Fluids: from Ultracold Quantum Gases to QCD Plasmas*, A. Adams, L. D. Carr, T. Schaefer, P. Steinberg, J. E. Thomas (eds.).
[8] S. Tan, Ann. Phys. **323**, 2952 (2008).
[9] S. Tan, Ann. Phys. **323**, 2971 (2008).
[10] E. Braaten, Lecture Notes in Physics **836**, 193 (2012).
[11] Y. Castin and F. Werner, Lecture Notes in Physics **836**, 127 (2012).
[12] E. Braaten and L. Platter, Phys. Rev. Lett. **100**, 205301 (2008).
[13] G. B. Partridge, K. E. Strecker, R. I. Kamar, M. W. Jack, and R. G. Hulet, Phys. Rev. Lett. **95**, 020404 (2005).
[14] F. Werner, L. Tarruell, and Y. Castin, Eur. Phys. J. B **68**, 401 (2009).
[15] E. D. Kuhnle, H. Hu, X.-J. Liu, P. Dyke, M. Mark, P. D. Drummond, P. Hannaford, and C. J. Vale, Phys. Rev. Lett. **105**, 070402 (2010).
[16] E. D. Kuhnle, S. Hoinka, P. Dyke, H. Hu, P. Hannaford, and C. J. Vale, Phys. Rev. Lett. **106**, 170402 (2011).
[17] S. Hoinka, M. Lingham, K. Fenech, H. Hu, C. J. Vale, J. E. Drut, and S. Gandolfi, Phys. Rev. Lett. **110**, 055305 (2013).
[18] J. T. Stewart, J. P. Gaebler, T. E. Drake, and D. S. Jin, Phys. Rev. Lett. **104**, 235301 (2010).
[19] N. Navon, S. Nascimbène, F. Chevy, and C. Salomon, Science **328**, 729 (2010).
[20] W. Schneider and M. Randeria, Phys. Rev. A **81**, 021601(R) (2010).
[21] Y. Sagi, T. E. Drake, R. Paudel, and D. S. Jin, Phys. Rev. Lett. **109**, 220402 (2012).
[22] F. Palestini, A. Perali, P. Pieri, and G. C. Strinati, Phys. Rev. A **82**, 021605(R) (2010).
[23] T. Enss, R. Haussmann, and W. Zwerger, Ann. Phys. **326**, 770 (2011).
[24] H. Hu, X.-J. Liu, and P. D. Drummond, New J. Phys. **13**, 035007 (2011).
[25] J. E. Drut, T. A. Lähde, and T. Ten, Phys. Rev. Lett. **106**, 205302 (2011).
[26] K. Van Houcke, F. Werner, E. Kozik, N. Prokof'ev, B. Svistunov, M. J. H. Ku, A. T. Sommer, L. W. Cheuk, A. Schirotzek, and M. W. Zwierlein, Nature Phys. **8**, 366 (2012).
[27] K. Van Houcke, F. Werner, E. Kozik, N. Prokof'ev, and B. Svistunov, *to be submitted to Phys. Rev. B.*
[28] P. Pieri, A. Perali, and G. C. Strinati, Nature Physics **5**, 736 (2009).
[29] R. Haussmann, M. Punk, and W. Zwerger, Phys. Rev. A **80**, 063612 (2009).
[30] F. Werner and Y. Castin, Phys. Rev. A **86**, 013626 (2012).
[31] R. Haussmann, Phys. Rev. B **49**, 12975 (1994).
[32] Z. Yu, G. M. Bruun, and G. Baym, Phys. Rev. A **80**, 023615 (2009).
[33] X. Leyronas, Phys. Rev. A **84**, 053633 (2011).
[34] O. Goulko and M. Wingate, Phys. Rev. A **82**, 053621 (2010).
[35] M. Ku, A. Sommer, L. W. Cheuk, and M. W. Zwierlein, Science **335**, 563 (2012).
[36] G. C. Strinati, Lecture Notes in Physics **836**, 99 (2012).
[37] R. Haussmann, W. Rantner, S. Cerrito, and W. Zwerger, Phys. Rev. A **75**, 023610 (2007).
[38] H. Hu, X.-J. Liu, and P. D. Drummond, Phys. Rev. A **77**, 061605(R) (2008).
[39] R. Combescot, F. Alzetto, and X. Leyronas, Phys. Rev. A **79**, 053640 (2009).
[40] S. Gandolfi, K. E. Schmidt, and J. Carlson, Phys. Rev. A **83**, 041601(R) (2011).
[41] D. T. Son and E. G. Thompson, Phys. Rev. A **81**, 063634 (2010).
[42] E. Taylor and M. Randeria, Phys. Rev. A **81**, 053610 (2010).
[43] W. D. Goldberger and I. Z. Rothstein, Phys. Rev. A **85**, 013613 (2012).
[44] Y. Nishida, Phys. Rev. A **85**, 053643 (2012).
[45] M. Punk and W. Zwerger, Phys. Rev. Lett. **99**, 170404 (2007).
[46] G. Baym, C. J. Pethick, Z. Yu, and M. W. Zwierlein, Phys. Rev. Lett. **99**, 190407 (2007).